ACS APPLIED MATERIALS & INTERFACES

Research Article

www.acsami.org

Dramatic Enhancement in Photoresponse of β-In_2S_3 through Suppression of Dark Conductivity by Synthetic Control of Defect-Induced Carrier Compensation

Nilima Chaudhari,*[†] Lily Mandal,[⊥] Onkar Game,[⊥] Sambhaji Warule,[‡] Deodatta Phase,[§] Sandesh Jadkar,*[†] and Satishchandra Ogale*[⊥]

[†]Department of Physics, Savitribai Phule Pune University, Pune 411007, India

[‡]Department of Physics, Nowrosjee Wadia College, Pune 411001, India

[§]UGC-DAE Consortium for Scientific Research, University Campus, Indore 452001, India

[⊥]Centre of Excellence in Solar Energy, Physical and Materials Chemistry Division, National Chemical Laboratory (CSIR-NCL), Pune 411008, India

Supporting Information

ABSTRACT: We report on the synthesis of dense and faceted indium sulfide (β-In_2S_3) nano-octahedron films on fluorine-doped tin oxide-coated glass by the hydrothermal method and their photoresponse properties in a flip chip device configuration. We have examined the temporal evolution of the phase constitution, morphology, and optoelectronic properties for films obtained after growth interruption at specific intervals. It is noted that, initially, an $In(OH)_3$ film forms, which is gradually transformed to the β-In_2S_3 phase over time. In the case of the film wherein most, but not all, of $In(OH)_3$ is consumed, an exceptionally large photoresponse (light to dark current ratio) of ~10^4 and response time(s) (rise/fall) of ~88/280 ms are realized. This superior performance is attributed to nearly complete carrier compensation achievable in the system under high pressure growth leading to dramatic reduction of dark conductivity. It is argued that the temporally growth-controlled equilibrium between quasi-In interstitials and cation vacancies dictates the optoelectronic properties.

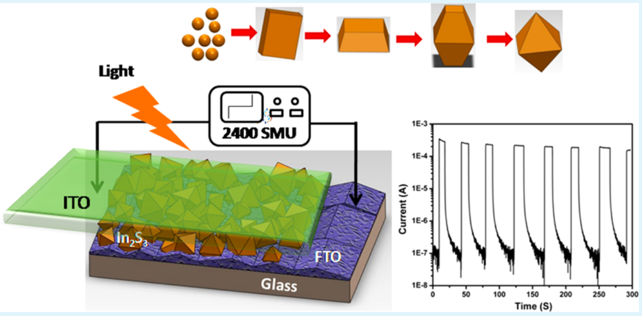

KEYWORDS: *β-In_2S_3, octahedrons, hydrothermal growth, photoresponse, defects, photoluminescence*

1. INTRODUCTION

Shape-controlled growth of semiconductor nanocrystals through a hierarchical assembly process has attracted significant scientific attention lately because of the size-, shape-, and morphology-dependent properties of nanomaterials that are key to various applications. It is further recognized that such interesting properties also depend greatly on the synthesis and processing methods because many atomistic aspects of the constitution of nanomaterials are influenced by material growth protocols and conditions.[1] Therefore, the development of precise architectures of nanomaterials with well-defined morphologies remains an important research endeavor.[2] This includes experimental design and controlled fabrication of high-index faceted nanocrystal forms that are chemically and electronically more functional or active.

Among the different chalcogenide semiconductors, indium sulfide (In_2S_3) is an n-type III−VI group chalcogenide semiconductor that has very promising optoelectronic properties. Furthermore, its band gap is well within the visible region (2−2.45 eV). There are three different crystalline phases of indium sulfide, namely, α (defect cubic), β (defect spinel), and γ (layered form), which stabilize depending on the processing conditions, especially temperature. Because of its versatile nature, In_2S_3 is widely explored for many different kinds of applications, such as photocatalysis, photoconductors, cancer diagnoses, color televisions, solid state batteries, and so forth.[1,3−7] It has also been synthesized in various morphologies, including nanotubes, nanowires, nanorod arrays, nanosheets, microflowers, nanoplates, single crystals, and thin films by using several methods.[8−14]

In the context of the present work, which deals with the study of photoresponse in β-In_2S_3, only a very few nanostructures and morphologies of this material have been utilized thus far,[11−13,15] most likely because achieving a strong attachment of In_2S_3 nanostructure of well-defined morphology on a conducting substrate is a formidable challenge.[16,17] To this end, hydro-

Received: April 5, 2015
Accepted: July 30, 2015
Published: July 30, 2015

© 2015 American Chemical Society

DOI: 10.1021/acsami.5b02885
ACS Appl. Mater. Interfaces 2015, 7, 17671−17681

Scheme 1. Energy Band Diagram of FTO, In_2S_3, and ITO along with the Device Schematic

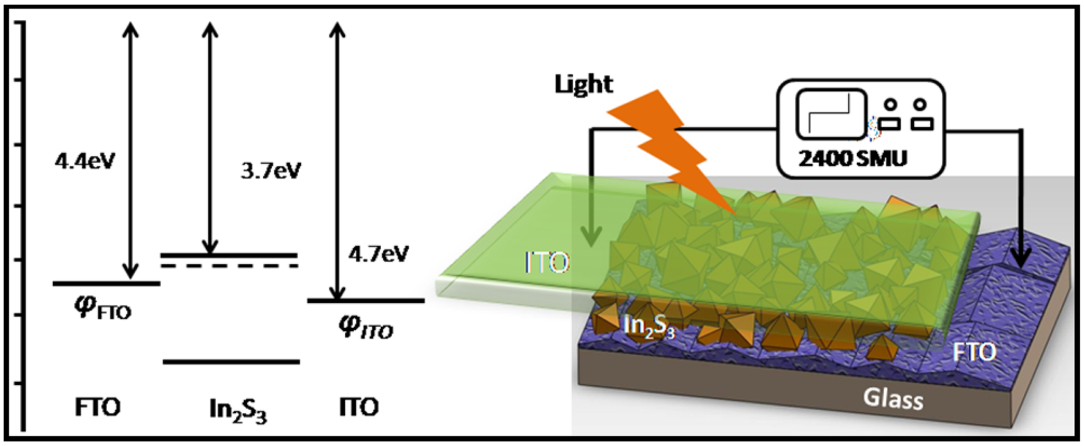

thermal synthesis offers a distinct advantage over the other methods because it not only renders the desired morphologies of inorganic materials on a substrate in a single step, but in light of the specific high pressure (superheating) growth character, adherent films of high crystalline quality can be grown fairly easily. Thus, in the present work, we have synthesized high index faceted and adherent β-In_2S_3 nano-octahedron coatings on FTO-coated glass substrates via a facile hydrothermal route. The effect of hydrothermal processing duration on the phase evolution of β-In_2S_3 has also been systematically studied. For the optimized conditions, wherein a small amount of $In(OH)_3$ coexists with the major phase component of β-In_2S_3, a very high photosensitivity (I_{light}/I_{dark}) of $\sim 10^4$ is realized in our films under a bias of 1 V. In other studies, coexistence of these two phases has indeed been shown to lead to superior photocatalytic activities.[18,19] We have also seen that the photoresponse in the optimally hydrothermally processed sample is far too strong compared to that observed in the conventionally synthesized film of pure β-In_2S_3 by ex situ sulfurization of $In(OH)_3$. This sulfurization synthesis[20,21] was adopted in this work specifically to bring out the significance of the hydrothermal method vis a vis the conventional synthetic approaches in the context of the specific photosensing application. As discussed later, the synthesis approach controls the nature of defect states in the final material in addition to its crystallinity and morphology, and in the case of semiconductors, these states play a key role in optoelectronic phenomena.

2. EXPERIMENTAL SECTION

2.1. Synthesis of In_2S_3 Films via Hydrothermal Method. All chemicals used in the synthesis were of AR grade and used without any kind of purification. In_2S_3 films are prepared on fluorine-doped tin oxide (FTO) glass substrates by an in situ hydrothermal synthesis technique. For this, indium nitrate is used as the indium (In) precursor, and thiourea is used as the sulfur (S) precursor. In a typical synthesis, indium nitrate (2 mmol) and double excess (6 mmol) of thiourea are dissolved under constant stirring in 75 mL of DI water. Then, the solution is vigorously stirred for 30 min. This solution is then transferred into a Teflon liner with 100 mL capacity. The FTO-coated glass substrates are cleaned and dried at 450 °C for 2 h. These are then tied to Teflon tape and properly hung into the reactor. The autoclave is kept in the oven at 160 °C for different durations of time (from 2 to 24 h), and the samples are then recovered in each case. The purpose of different hydrothermal durations (i.e., 2, 6, 10, 16, 24 h, etc.) was to understand details about the phase formation and morphology evolution.

The sample formed after 2 h was comprised of only the $In(OH)_3$ phase, whereas the sample obtained after 10 h primarily contained the β-In_2S_3 phase with a small residual $In(OH)_3$. The sample obtained after 24 h contained only β-In_2S_3. In all cases, the reactor is naturally cooled to room temperature. The film obtained after 10 h exhibited a strong response as discussed later. This case of an orange-colored film uniformly coated on the FTO substrate is labeled as H_{10}-In_2S_3 and is the main material of interest because of its lowest dark conductivity feature. The other case of the film obtained after 24 h is denoted by H_{24}-In_2S_3. All films are further washed 2−3 times with DI water and ethanol. Finally, these are dried in a vacuum and used for further characterization. To elucidate the role of $In(OH)_3$ in defining the state of the H_{10}-In_2S_3 sample on the photoresponse, we compared different results with the hydrothermally synthesized film for a reaction period of 24 h (H_{24}-In_2S_3; pure β-In_2S_3) and the β-In_2S_3 film made by ex situ sulfurization of $In(OH)_3$, leading to the sample identified as S-In_2S_3.

2.2. Synthesis of In_2S_3 Films via Sulfurization (S-In_2S_3). As stated above, we also synthesized In_2S_3 films on FTO substrates by ex situ sulfurization of $In(OH)_3$ films at higher temperature. For this, first, $In(OH)_3$ films are synthesized on FTO substrates using the hydrothermal method and are then kept in a tubular furnace. For sulfurization, argon gas is passed through the trap containing thioacetamide as a sulfur precursor. The furnace is set at 400 °C at a heating rate of 5 °C/min. The film is kept for 30 min at 400 °C and cooled naturally. An orange-colored film is thus obtained and is labeled S-In_2S_3.

2.3. Characterization. The samples are characterized by X-ray diffraction using a Philips X'Pert PRO diffractometer with nickel-filtered Cu K_α radiation for structural phase determination. The morphological study of the samples is carried out using scanning electron microscopy (FEI Nova NANOSEM 450), whereas the detailed atomistic structural quality is determined using high resolution transmission electron microscopy (IFEI, Tecnai F30, FEG system with 300 kV). The chemical analysis of the as-synthesized In_2S_3 film is carried out using X-ray photoelectron spectroscopy (VG scientific ESCA-3000 spectrometer using non-monocromatized Mg K_α radiation (1253 eV) at a pressure of $\sim 1 \times 10^{-9}$ Torr. The band gap of the material is determined by diffuse reflectance spectroscopy (DRS). Photoluminescence (PL) studies are carried out using FLS 980 (Edinburgh Instruments). The attenuated total reflection-Fourier transform infrared spectroscopy (ATR-FTIR) is recorded on a JASCO FT/IR-6100 spectrometer. The *I*−*V* characteristics are recorded with a Keithley 2420 source measuring unit. To measure the photoresponse, a solar simulator (Newport, AM1.5, 100 mW cm^{-2}) is used.

2.4. Device Fabrication. In the device configuration, the FTO-coated glass on which the indium sulfide film is grown acts as the bottom electrode and is connected to the ground. ITO-coated glass is used as the transparent top electrode and connected to the terminal of the power supply. The flip chip method is used to make the device. For the measurement of photoresponse properties, the light is irradiated through the transparent (ITO) side of the flip chip geometry (as shown in Scheme 1).

3. RESULTS AND DISCUSSION

3.1. X-ray Diffraction (XRD). Figure 1 depicts the X-ray diffraction (XRD) patterns of (a) an FTO substrate, (b and c) In_2S_3 films grown on an FTO substrate by 10 h (H_{10}-In_2S_3), and 24 h hydrothermal reactions (H_{24}-In_2S_3). Figure 1d is for the In_2S_3 film grown on an FTO substrate by the sulfurization method (S-In_2S_3). All three XRD patterns (H_{10}-In_2S_3, H_{24}-In_2S_3, and S-In_2S_3) exhibit a set of well-defined diffraction peaks, indicating tetragonal β-In_2S_3 phase with lattice constants of a = b = 7.623 Å and c = 32.36 Å, in good agreement with the reported values (JCPDS Card No. 73−1366). Additionally, the diffraction peaks corresponding to $In(OH)_3$ phase (JCPDS card No. 85−1338, marked by *) can be seen only in the XRD of H_{10}-In_2S_3.

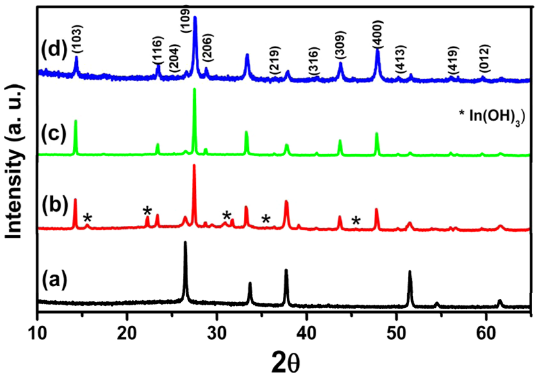

Figure 1. XRD patterns of (a) FTO substrate, (b) In_2S_3 film on FTO obtained after 10 h and (c) 24 h hydrothermal reactions; d) In_2S_3 film on FTO obtained by the sulfurization method (S-In_2S_3).

To study the formation and transformation of $In(OH)_3$, hydrothermal reactions for different durations (2, 7, 10, 16, and 24 h) were carried out. After a 2 h reaction, a completely white film of $In(OH)_3$ is obtained (please see Figure SI-1a). Hence, it is clear that, in the case of hydrothermal synthesis, first indium hydroxide formation takes place and then it is converted to In_2S_3. For 6 h of hydrothermal reaction time (H_6-In_2S_3), small peaks of β-In_2S_3 phase are noted in addition to those of the $In(OH)_3$ phase (Figure SI-1b). As the reaction proceeds further (10 h case), the growth of β-In_2S_3 becomes more predominant in comparison to that of the $In(OH)_3$ phase (Figure 1b). The contribution of indium hydroxide is observed to be negligible in the case of 16 h hydrothermal synthesis (Figure SI-1d). Further increasing the reaction time up to 24 h leads to the formation of pure β-In_2S_3 phase (Figure 1c). Also, in the case of the sulfurized film, $In(OH)_3$ is completely converted to indium sulfide (Figure 1d) after 30 min of sulfurization at 400 °C. No signatures of hydroxide are observed in this case either. As shown and discussed later, the presence of $In(OH)_3$ in defining the corresponding state of the sample makes a huge difference in the photoresponse behavior of the three cases (H_{10}-In_2S_3, H_{24}-In_2S_3 and S-In_2S_3). In light of the presence of textures (selected plane orientations) and changes in grain size-dependent line widths in the film, it is nontrivial to extract precise information about phase constitution. A rough estimate based on the heights of the maximum intensity peaks for the two phases (β-In_2S_3 and $In(OH)_3$) is provided in Figure SI-2.

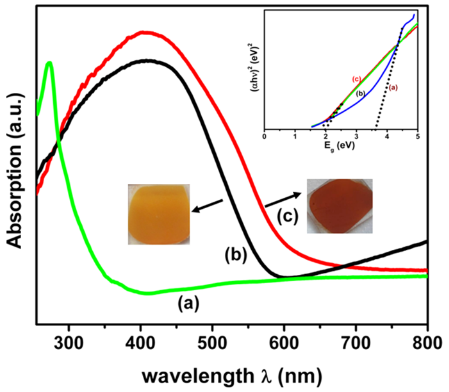

Figure 2. UV−vis DRS spectra of (a) $In(OH)_3$, (b) H_{10}-In_2S_3, and (c) S-In_2S_3 film samples. Inset depicts Tauc plots for the three cases.

3.2. UV-DRS Spectroscopy. Figure 2a displays the UV−vis diffuse reflectance spectra (DRS) for the $In(OH)_3$ film obtained after a 2 h hydrothermal reaction. This film, which is white in appearance due to scattering, shows absorption in the range of 290−340 nm. Panels b and c in Figure 2 depict the UV−vis DRS spectra for the In_2S_3 films on an FTO substrate synthesized by the hydrothermal reaction (H_{10}-In_2S_3) and sulfurization method (S-In_2S_3), respectively. Both the In_2S_3 samples show broad band absorption in the visible region (400−600 nm). The H_{10}-In_2S_3 film shows an absorption edge at ∼600 nm, whereas S-In_2S_3 shows a relative red shift in the absorption edge (∼650 nm). The contribution of $In(OH)_3$ (absorption in the range of 290−340 nm) causes the H_{10}-In_2S_3 sample to appear orange, whereas its absence in the S-In_2S_3 sample renders it a dark brown color. It is clearly seen that both the In_2S_3 films show a steep absorption edge in the visible region, which is attributed to the intrinsic transition of In_2S_3 (with the possibility of In deficiency shifting bands vis a vis each other). The optical energy band gap values for $In(OH)_3$, H_{10}-In_2S_3, and S-In_2S_3 films calculated from Tauc's plot using UV-DRS data are found to be ∼3.6, 2, and 1.78 eV, respectively.

3.3. Field Emission Scanning Electron Microscopy (FESEM). To reveal the surface morphology of as-synthesized films (H_{10}-In_2S_3 and S-In_2S_3), FESEM images were recorded, and the same are displayed in Figure 3. The morphology of H_{10}-In_2S_3 deposited on the FTO substrate (Figure 3a, b) clearly shows a distribution of very well-defined and faceted octahedrons on the substrate. The size of the octahedron is observed to be ∼200 nm. It can be seen that the edges of the octahedron-shaped individual grains in this coating are sharp, and the corresponding surface facets are smooth on the scale of resolution of the image (see Figure 3b inset). Conversely, the sulfurized film sample (S-In_2S_3) shows irregularly shaped particulate morphology (Figure 3c, d). Because of the higher sulfurization temperature (400 °C) and the reactive nature of the transformation process from $In(OH)_3$ to In_2S_3, the particles are agglomerated in such a way that they form clusters of In_2S_3.

It may be noted that this agglomeration or shape evolution is caused by the reactive aspect of the sulfurization process and not physical melting or related shape transformation of the sample. The chemical reactions, especially when large density changes are involved, involve significant mass flow, yielding opportunities for fusing of interfaces and shape evolution even at reasonable temperatures. Moreover, the reaction rates are different along different crystallographic directions. The temporal growth evolution (phase and morphology) leading to the final faceted state in the case of the hydrothermal process was also examined and is brought out with the help of the XRD and FESEM characterizations on the samples obtained after different reaction times. (see Figure SI-3A, B).

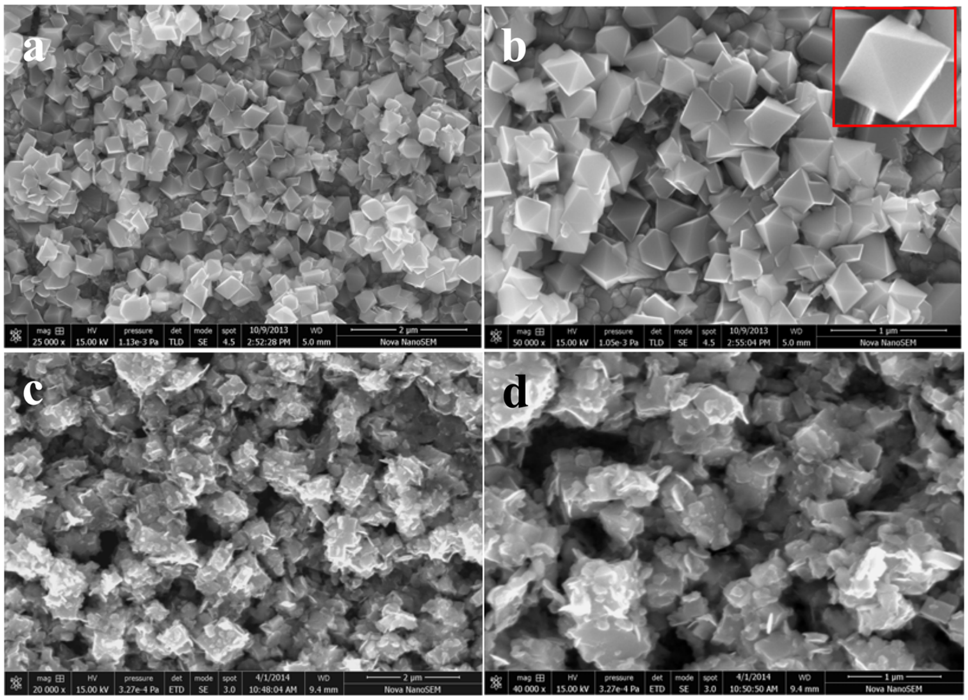

Figure 3. FESEM images of In_2S_3 synthesized via the (a, b) hydrothermal (H_{10}-In_2S_3) and (c, d) sulfurization (S-In_2S_3) method.

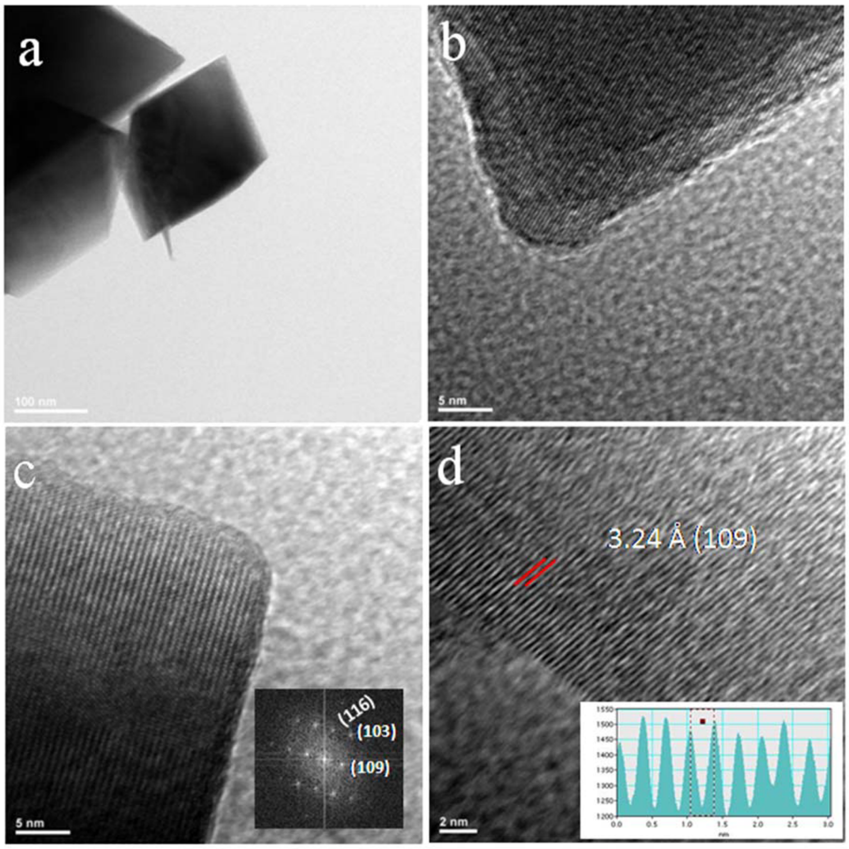

Figure 4. (a, b) TEM and (c, d) HRTEM images of hydrothermally grown In_2S_3 octahedrons in H_{10}-In_2S_3. Inset of (c) is the FFT pattern of the respective image, which is marked.

3.4. Transmission Electron Microscopy (TEM). Transmission electron microscopy (TEM) was employed to understand the crystallographic facets and the well-defined morphology of the In_2S_3 octahedron in the case of the H_{10}-In_2S_3 sample. Figure 4a displays a typical TEM image of such an octahedron morphology. These octahedrons consist of fairly sharp facets, and the contrast variation is observed from the edge to the center due to the thickness effect in imaging due to the pyramid-shaped

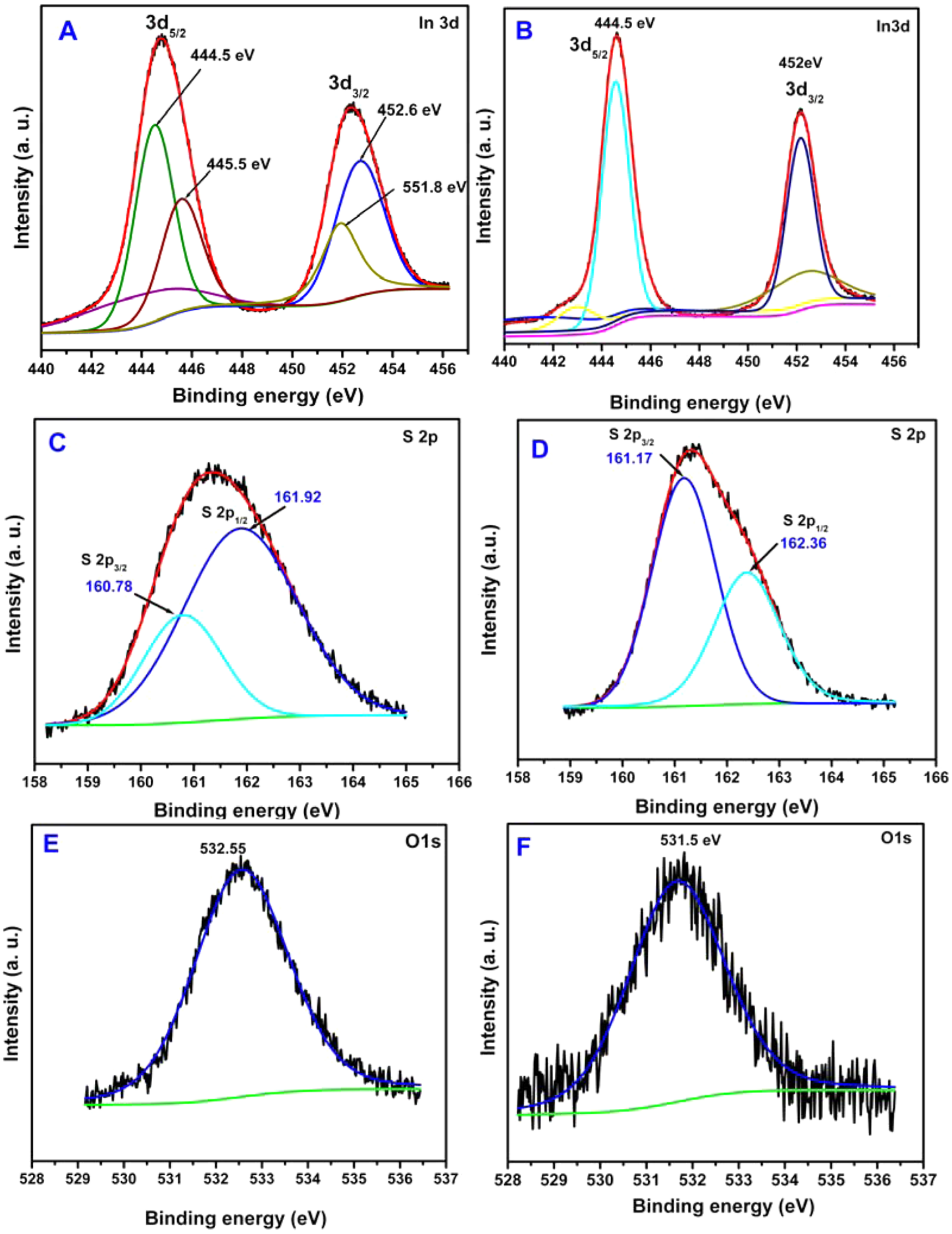

Figure 5. (A, B) In_{3d} core level spectra, (C, D) S_{2p} spectra, and (E, F) O 1s spectra for the H_{10}-In_2S_3 and S-In_2S_3 samples, respectively.

morphology. The side edge length of the pyramid is found to be ~120 nm. Panels b−d in Figure 4 show high-resolution TEM (HRTEM) images obtained from the edge of the β-In_2S_3 octahedron, which indicate a defect-free single crystalline nature of the material. The calculated atomic spacing is observed to be ~3.24 Å, which corresponds to the highest intensity (109) planes (JCPDS Card No. 73-1366). The inset of Figure 4c is a typical FFT pattern, which again indicates that the product is highly single crystalline in nature.

3.5. X-ray Photoelectron Spectroscopy (XPS). XPS analysis was carried out to study the electronic states of the In, S, and O ions in the samples synthesized via hydrothermal and sulfurization methods. All the spectra are calibrated using the C(1s) reference of 284.6 eV. The Shirley procedure was used to define the background of the spectra. The comparison of deconvoluted In_{3d} high resolution core level spectra for H_{10}-In_2S_3 and S-In_2S_3 are shown in Figure 5A and B, respectively.

It may be noted that no significant asymmetry is seen in either of these spectra, although the spectral width in the case of the H_{10}-In_2S_3 sample is much broader (fwhm ~2.4 eV) than that of the S-In_2S_3 sample (fwhm ~1.38 eV), signifying the possibility of multiphase contributions or the presence of defects in the case of the H_{10}-In_2S_3 sample. In this H_{10}-In_2S_3 sample, the deconvoluted $In_{3d5/2}$ core level spectrum contains a peak at 445.5 eV (Figure 5A), which can be attributed to the indium in the hydroxide form.[22] This may represent the residual $In(OH)_3$ in the sample seen in the XRD. Such a peak is absent in the case of the S-In_2S_3 sample, as expected. The deconvoluted spectrum for H_{10}-In_2S_3

shows another $In_{3d5/2}$ contribution at 444.5 eV, which corresponds to the β-In_2S_3 phase, though its fwhm is 1.81 eV (much higher than the corresponding contribution in S-In_2S_3, which has a fwhm of 1.38 eV). The broadening of the peaks can be the result of surface charging, which could be attributed to the adsorbed groups[23] or the presence of specific defect states (e.g., Indium interstitials or quasi-interstitials). Biswas et al.[24] have also noted such a contribution in their sol−gel derived films, and this contribution was seen to vanish after surface cleaning by sputtering. This made the authors assign this contribution to free surface hydroxyl groups. Both of these factors (surface groups and defects) could lead to electronic effects via the introduction of electronic states or carrier doping effects. Some of these aspects are reflected in the discussion pertaining to the photoluminescence data presented and discussed in later sections.

In addition to this, the spectra of S_{2p} in both of the samples (Figure 5C, D) show broad peak contributions and can be deconvoluted into two peaks for S $2p_{3/2}$ and S $2p_{1/2.}$ The binding energy values in the case of the H_{10}-In_2S_3 sample are shifted to lower energies (161.9 and 160.78 eV) than the binding energies for the sulfurized S-In_2S_3 sample (162.3 and 161.17 eV). This may be due to the adsorbed hydroxide groups in the hydrothermally synthesized sample.

In the case of the O 1s spectrum for the H_{10}-In_2S_3 sample, the binding energy is observed at 532.5 eV (Figure 5E). This value is characteristic of oxygen in the hydroxyl form (−OH).[25] Conversely, in the case of the S-In_2S_3 sample, the binding energy is observed at 531.5 eV (Figure 5F), which is attributed to adsorbed oxygen.[25] The difference in binding energy of the O 1s spectra in In-OH and adsorbed oxygen is due to the change in the electrostatic interaction. There are on average fewer electrons on the oxygen atom in In-OH than in the In-adsorbed oxygen case because of higher electronegativity of hydrogen than indium. This causes the binding energy of the electrons to increase, leading to a shift of the binding energy in the O 1s spectra to a higher value in the H_{10}-In_2S_3 sample. This supports the presence of hydroxyl groups on the surface of this sample.[26] This conforms with the inference drawn from the nature of In_{3d} contributions.

From the XPS study, it is observed that all of the In, S, and O ions are surrounded by hydroxyl groups in the case of the H_{10}-In_2S_3 sample, whereas these signatures are absent in XPS spectra of the S-In_2S_3 sample. This is a further evidence of the presence of some quantity of $In(OH)_3$ in the 10 h hydrothermally synthesized In_2S_3 sample (H_{10}-In_2S_3). These results are clearly in good agreement with the XRD results, and as discussed next, are also supported by the ATR-FTIR spectroscopy study.

3.6. ATR-FTIR Study. To confirm the contribution of hydroxyl functional groups in the case of the hydrothermally synthesized sample, ATR-FTIR studies were carried out on both the H_{10}-In_2S_3 and S-In_2S_3 samples (Figure 6a, b).

It is clearly seen that the strong peaks at 3300 and 1625 cm^{-1} in the hydrothermally grown sample H_{10}-In_2S_3 (Figure 6a) are attributable to the adsorbed hydroxyl groups (−OH bonding).[27,28] These peaks are almost absent in the case of sulfurized In_2S_3 film sample S-In_2S_3 (Figure 6b). Additionally, the presence of a small IR band at 1107 cm^{-1} in H_{10}-In_2S_3 is due to the vibrational frequency of ν(S−O) bond in SO_4^{2-}.[29] IR bands are observed at 778 and 1033 cm^{-1} in both the cases and are attributable to the (S−O) stretching frequency.[30] In the case of S-In_2S_3, the IR bands at 665, 1407, and 1597 cm^{-1} are attributed to the C═S, C−N, and $-CH_3$ stretching frequencies, respectively.[31] These bands originate from the thioacetamide used in the sulfurization process.

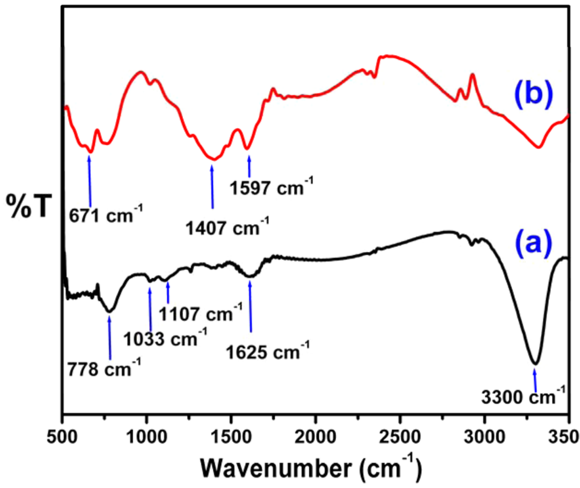

Figure 6. ATR-FTIR spectra of In_2S_3 films deposited on FTO-coated glass substrates with (a) H_{10}-In_2S_3 and (b) S-In_2S_3.

Thus, the XRD, XPS, and ATR-FTIR techniques all collectively confirm the presence of hydroxyl groups in the hydrothermally deposited H_{10}-In_2S_3 sample. Conversely, these groups are absent in the S-In_2S_3 sample synthesized by the sulfurization method. It is well reported that the presence of hydroxyl groups on the surface increases the charge (e^-/h^+) separation property of the respective semiconductor.[32] The charge separation becomes faster with an increasing number of surface hydroxyl groups. According to the evidence in previous reports, the surface OH^- ions form hydroxyl radicals (OH•) by capturing the photoinduced holes (h^+). This process restricts the recombination of electron/hole (e^-/h^+) pairs, which results in the enhancement of the photocatalytic activity.[27,32] This phenomenon is also found to be useful in other optoelectronic devices.[33] In the present study, we used the synthesized film samples for photosensing applications and indeed observed an interesting influence of the synthesis route, hydroxyl ion contribution, and morphological difference on the photoresponse properties.

3.7. Electrical and Optoelectronic Properties of FTO-Indium Sulfide-ITO Flip Chip Device. The junction between indium sulfide grown on FTO and ITO counter electrodes was made by the simple flip chip method (top press contact). Here, ITO-coated glass is the front contact and In_2S_3 deposited FTO glass is the back contact of the device.

In this work, we have compared the photoresponse properties of H_{10}-In_2S_3 synthesized by the hydrothermal and the sample synthesized by the sulfurization method (S-In_2S_3). The $I-V$ characteristics of the devices were studied in CPP (current perpendicular to plane) configuration. The dark/light (AM 1.5 1 Sun 100 mW/cm^2) $I-V$ characteristics of the H-In_2S_3 and S-In_2S_3 devices are shown in Figure 7a and b, respectively. The typical photoresponse (in terms of current) as a function of time is shown in Figure 7c and d for H_{10}-In_2S_3 and S-In_2S_3, respectively.

It is seen that the devices show rectifying behavior with a rectification ratio ($I_{forward}/I_{reverse}$) of 100 at ±1 V. It may be noted that over the range from −0.7 to +1.0 V, the current is extremely small (less than $\sim 3 \times 10^{-8}$ A) and is noisy. Below −0.7 V, it rises as the applied bias is reduced to −1.0 V. Referring to Scheme 1, it is interesting that the band offset between FTO and β-In_2S_3 is 0.7 V on one side, whereas between ITO and β-In_2S_3 on the other

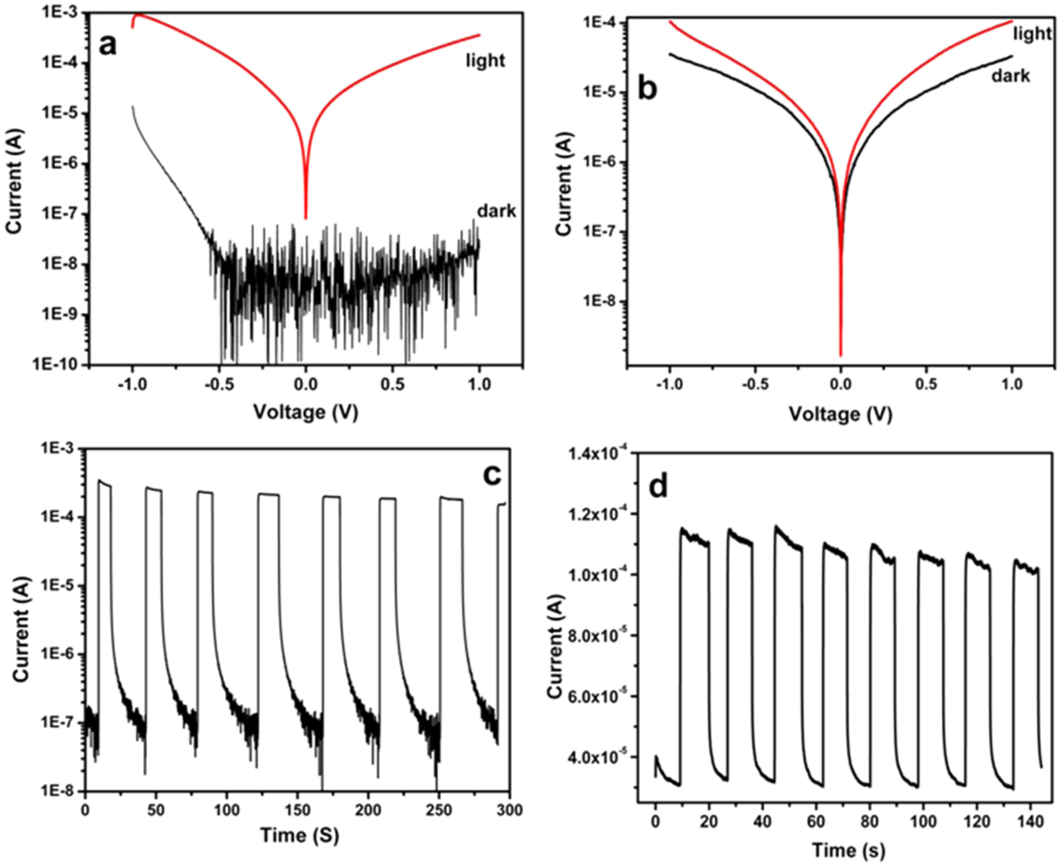

Figure 7. *I*−*V* curves in the dark (black) and illuminated (red) for (a) H_{10}-In_2S_3 and (b) S-In_2S_3 photodetectors. The photoresponse as a function of time with light chopping at 1 V bias for (c) H_{10}-In_2S_3 and (d) S-In_2S_3films.

side, it is 1.0 V.,[18,34] This can lead to the generation of asymmetric Schottky barriers due to electron transfer across the interfaces. Moreover, the conduction band of $In(OH)_3$ is only 0.13 eV below that of β-In_2S_3,[35] hence, such a layer would not change this physical picture significantly even if present as a residual phase. A similar kind of rectifying behavior was also reported in vertically aligned In_2S_3 nanowires with gold (Au) contacts,[9] and the rectification was attributed to the difference in the work functions of In_2S_3 and Au (the electrons getting injected from In_2S_3 into the Au electrode). Under the illumination of light on the device made on the H_{10}-In_2S_3 sample (10 h hydrothermal reaction), a photoresponse (I_{light}/I_{dark}) of ~10^4 is seen (Figure 7a). In contrast to this, the device made using the S-In_2S_3 film shows a much smaller (factor of only 3) photoresponse (Figure 7b).

Panels c and d in Figure 7 show the photocurrent response as a function of time for the H_{10}-In_2S_3 and S-In_2S_3 devices, respectively. It is useful to mention here that the photoresponse was evaluated for all cases of hydrothermally synthesized samples (6, 10, 16, and 24 h), and the response for the 10 h case was found to be significantly higher than for the other cases (see Figure SI-4). Hence, we focus on the same for the discussion here. Interestingly, the H_{10}-In_2S_3 device shows 4 orders of magnitude photoresponse (10000×) in the presence of light as compared to that of the S-In_2S_3 device, which shows only a factor of 3.

The applied bias voltage influences the on/off ratio of the devices, which is the result of the applied bias voltage dependence of the exciton dissociation and the background current of the device. The Off and On current values for the device are almost the same for different light chopping cycles, indicating the photostability and reversibility of the device. The dynamic photoresponse properties of the devices are measured by applying a constant potential of 1 V and chopping the light source. The rise time is defined as the time taken by the photocurrent to reach 90% of its maximum value, and the reset (recovery) time is the time taken by the maximum photocurrent to reduce down to 10% upon terminating the light exposure. The rise/reset times for S-In_2S_3 and H_{10}-In_2S_3 are 88/280 and 160 ms/4 s, respectively, as shown in Figure SI-5.

We also estimated the photoconducting gain for the optimum (H_{10}-In_2S_3) case. The corresponding procedure, calculations, and numbers are given in SI-6. The gain in our case is much lower than that achieved in the case of In_2S_3/Ag core−shell aligned nanorod array grown by the glancing angle deposition method,[15] and further work will be needed to design and engineer our device configuration for higher performance.

In a separate case, a device was made using the H_{24}-In_2S_3 film synthesized by a 24 h hydrothermal reaction in which single phase β-In_2S_3 phase formation was noted (i.e., without any discernible contribution of $In(OH)_3$). It showed a photoresponse (I_{light}/I_{dark}) factor of only 92 (Figure 8), which is far too low compared to that of the film synthesized in 10 h wherein β-In_2S_3 and $In(OH)_3$ coexisted.

As stated earlier, all of the intrinsic properties of In_2S_3 are essentially controlled by its defect structure.[1] In_2S_3 is known to have considerable concentration of cation vacancies. By furnishing a small amount of energy, the indium ions on the lattice site can be transferred to an ordered vacancy site. Therefore, a few In atoms may easily occupy crystallographically ordered vacancies by leaving their ordered positions to produce

DOI: 10.1021/acsami.5b02885
ACS Appl. Mater. Interfaces 2015, 7, 17671−17681

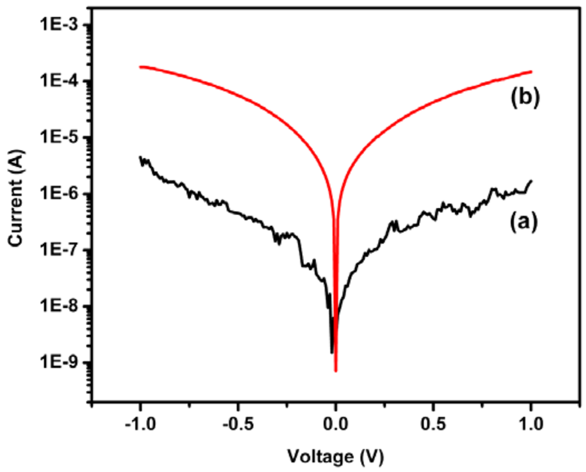

Figure 8. (a, b) *I*−*V* curves in the dark and under illumination for the H_{24}-In_2S_3 sample synthesized by the hydrothermal reaction for 24 h.

quasi-interstitial cations and disordered cation vacancies. The quasi-interstitial cations and disordered cation vacancy act as donor and acceptor, respectively. When indium sulfide is grown at high sulfur pressure or treated with sulfur after synthesis, then its resistivity is found to be very high as compared to indium sulfide grown by other methods, because it becomes a compensated semiconductor with nearly compensating quasi-interstitial cations and disordered cation vacancies.[1] Indeed, the equilibrium concentrations of ionized donors, acceptors, and thereby, electrons and holes, in In_2S_3 are known to depend strongly on sulfur pressure.

Given the significance of defect states in controlling the optoelectronic properties of this system, we subjected our samples to photoluminescence (PL) studies to explore and elucidate the possible signatures of defect states. The data for several cases of interest are shown in Figure 9. The excitation wavelength was kept fixed at 270 nm. The data are normalized to the peak intensity of the emission peak at 430 nm, which corresponds to the signature for the FTO substrate layer. Interestingly, the highest PL intensity is observed for the 10 h case (Figure 9A), which also shows the strongest photoresponse as discussed earlier. It also exhibits a structure comprised of some distinct contributions that are discussed next. The 6 h case also shows reasonable intensity along with a peak structure, but the intensity is lower in other cases. To decipher the individual contributions, we nominally fitted the PL data for the 10 h case with multiple peaks (Figure 9B). The data could be fitted fairly well with three contributions at 558 nm (2.2 eV), 596 nm (2.08 eV), and 645 nm (1.92 eV).

Jayakrishnan[36] et al. have precisely addressed the issue of different defect states in the β-In_2S_3 system by photoluminescence studies and have identified the energy states corresponding to sulfur vacancy, indium vacancy, indium interstitial, and the defect state formed by the oxygen atom

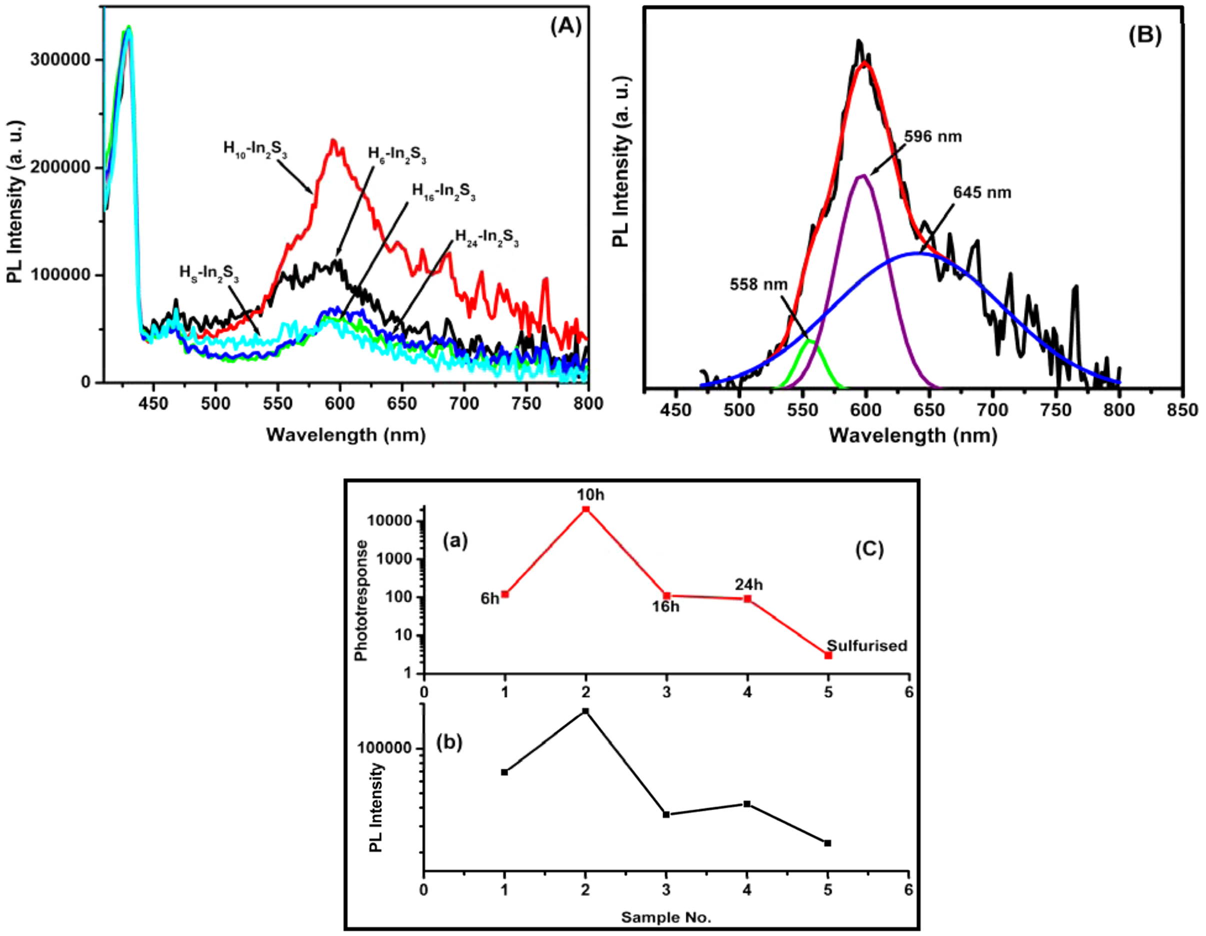

Figure 9. (A) Photoluminecence (PL) spectra of as prepared film samples, (B) fitted PL data for the H_{10}-In_2S_3 case, and (C) comparison of photoresponse and PL intensity for different samples.

DOI: 10.1021/acsami.5b02885
ACS Appl. Mater. Interfaces 2015, 7, 17671−17681

replacing sulfur vacancy. The sulfur vacancy and indium interstitial are donor defects, whereas the other two are acceptor defects. The sulfur vacancy and oxygen related states are deep states, whereas the other two are relatively shallow states.

The fitted peak at 558 nm (2.22 eV) corresponds to the A-band identified by Jayakrishnan,[33] which is attributed to the transition from the sulfur vacancy state to the acceptor level (indium vacancy in this case). The broad peak centered at ~645 nm (1.92 eV) corresponds to the transition from the indium interstitial donor state to the acceptor state emanating from oxygen replacing the sulfur vacancy. Finally, the main peak in our PL data for the 10 h case, corresponding to the transition at 596 nm (2.07 eV), was discussed by Jayakrishnan et al.[36] via fitting their rather broad spectrum for spray-coated film samples by multiple peaks. However, it was not definitively identified with any specific defect transition. Its prominence in samples prepared under indium-rich conditions made these authors conclude that this could be related to an indium interstitial-type defect. In our case, this contribution is quite distinct and intense. We believe that this may be due to the hydrothermal processing of our sample, vis a vis spray coating used by Jayakrishnan,[36] which can define the sample state differently. As discussed later, the notions of ordered cation vacancies and quasi-interstitials leading to local disorder in the ordered vacancy lattice can come into play in this system. These defects and defect complexes could have slightly different energies than cation interstitial and vacancy defects and may lead to slightly different transition energies in differently synthesized samples.

It is further very interesting to point out that the behavior of the photoresponse observed in different cases of interest almost mimics the PL intensity. This is shown in Figure 9C. Because the PL features directly emanate from the product of the specific donor and acceptor defect states, this drives home the point that the photoresponse systematic has a direct defect connection. This is discussed at some length in the paragraphs to follow.

It is now useful to comment on the possible reasons for the strong suppression of the dark conductivity in the case of the H_{10}-In_2S_3 sample and thereby the dramatic enhancement of the photoresponse. Summarizing the results, we basically have three cases that show differing dark conductivity as evidenced by the differences in the current flowing through the flip chip junction at the same applied voltage (e.g., 1 V). Because it is nontrivial to estimate the conductivity values quantitatively in the case of a flip chip junction, we make our arguments in terms of the systematic of the photoresponse (I_{light}/I_{dark} measured at +1 V bias) for the three stated cases, namely, (a) the sample that shows the lowest dark current (H_{10}-In_2S_3) obtained after 10 h of hydrothermal synthesis at 160 °C, (b) the sample that shows intermediate dark current that is also obtained by hydrothermal synthesis at 160 °C but after 24 h (H_{24}-In_2S_3) (Figure 8a, b), and (c) the third, which shows fairly high dark current after being obtained by ex situ sulfurization (S-In_2S_3) at high temperature (400 °C) starting from the single phase $In(OH)_3$ film obtained hydrothermally after just 2 h. Notably, the changes in dark current in the three cases are far more significant than the corresponding changes in the current under illumination. Therefore, the H_{10}-In_2S_3 sample, which shows lowest dark current (~10^{-8} A), shows the highest photoresponse under illumination as compared to the other two cases. These observations need to be analyzed in terms of the possible defect types incorporated under the stated three processing conditions because transport in this material is ultrasensitive to the growth conditions.

Long ago, Rehwald and Harbeke[1] had performed a very thorough study of the conduction mechanism in single crystal β-In_2S_3. Addressing a peculiar observation of an exponential increase in Hall mobility with temperature, they considered several possible mechanisms of conduction. This mainly included (a) the small polaron model with self-trapped charge carriers and the carrier motion occurring via a hopping process between localized states on lattice sites, (b) an interpretation based on an electrically inhomogeneous crystal with well-conducting regions imbedded in a matrix of high resistivity, and (c) a two carrier transport model with different scattering mechanisms for electrons and holes. On the basis of several careful measurements and analyses, they concluded that the two carrier model could explain most of their observations very well. They attributed the possible origin of the different scattering effects for electrons and holes to the differences in their effective masses with the local deformation potentials for lattice scattering and/or the cross-sections for impurity scattering. The results could be understood better in terms of predominant scattering of electrons by the impurities and holes by the lattice and, partially, the impurities. Shockley[37] argued that the wave function of an excess electron is concentrated in the vicinity of the cations and that of holes near the anions; hence, the scattering of a specific charge carrier type is primarily influenced by the disorder on the corresponding parent site. This makes the specific system very sensitive to the preparation route, and the properties such as the electrical resistivity and Hall coefficient can exhibit a remarkable range of over six decades. Given the key and significant role of separate sublattice disorders in β-In_2S_3, nonstoichiometry, if present or controlled, plays almost a defining role in its electronic and optical properties.

The β-modification of the In_2S_3 lattice (which is the observed phase in our samples) has a spinel structure, and the cation vacancies are randomly located on either the octahedral sites or both the octa- and tetrahedral sites. When the vacancies are ordered, the unit cell is comprised of three spinel cubes stacked along the *c*-axis in a tetragonal symmetry. In the ordered case, the vacancies cannot be regarded as the defects or scatterers but are part of the lattice defining the electronic band structure. However, if some cations leave their lattice position and occupy a vacancy site in an ordered vacancy lattice, quasi-interstitial cations are generated along with an equal number of disordered vacancies. In the case of β-In_2S_3, the energy to create such a defect complex is suggested to be low, and hence, even in a stoichiometric crystal, one can expect a fair degree of this type of disorder. Departure from stoichiometry can cause a surplus of interstitial cations or cation vacancies, which have to be compensated for by electrons and holes, respectively. Thus, interstitial cations serve as donors and cation vacancies as acceptors.

Rehwald and Harbeke[1] have argued using the equilibrium considerations based on the effect of temperature (thermal energy input), presence and pressure of sulfur, and so forth, that the concentration of quasi-interstitial indium and disordered vacancy defects (and thereby those of electrons and holes) will depend quite sensitively on the precise growth conditions. Under low sulfur conditions, the surplus of indium in the phase will favor higher concentration of quasi-interstitial indium over that of disordered vacancies leading to n-type conduction. At relatively higher sulfur pressure, the donors (electrons) and acceptors (holes) will nearly compensate for each other even though their individual concentrations could vary over several orders, a small residual concentration contributing to n-type conductivity will persist. Annealing in sulfur would add acceptors and reduce the residual n-type conduction. This scenario shows how the dark conductivity can be dramatically changed over several decades by proper tuning of the growth process.

Returning now to discuss the three cases of interest, in the case of H_{10}-In_2S_3, which exhibits the lowest dark conductivity, we still have residual $In(OH)_3$ phase coexisting with the desired β-In_2S_3 phase. Under this hydrothermal condition of high pressure and reasonable temperature, sulfur would primarily drive phase formation and not necessarily lead to the reduction of the quasi-In interstitial concentration. This would represent a condition where the donor concentration (and therefore the electron concentration) is high. Also, the incomplete or intermediate state of the phase conversion from $In(OH)_3$ to β-In_2S_3 would further imply that the cation vacancies would be more disordered, leading to a higher acceptor concentration as well. This means the condition is just right for an adequate and controlled decrease of the quasi-interstitial indium donor concentration to be close to the concentration of disordered vacancies, leading to high resistivity or extremely low dark conductivity (current). If we consider the second case of the sample recovered after 24 h from the hydrothermal autoclave (H_{24}-In_2S_3), the extended time would not only complete the full conversion of the remaining small amount of $In(OH)_3$ but would also help enhance the ordering of cation vacancies due to an annealing effect at 160 °C. The ordered vacancies contribute to the band states and would no longer serve as acceptors (defect states). This will decrease the hole concentration, causing enhanced n-type dark conductivity as observed. Finally, in the third case of sulfurization, one not only has a high and continuous flux of sulfur but also higher temperature (400 °C) than the hydrothermal processing temperature (160 °C). This will cause even further ordering of cation vacancies, thereby changing the defect equilibrium and rendering even higher n-type conductivity (higher dark current at 1 V) as also observed. Thus, by playing with the sample processing conditions, it is possible to tune the dark conductivity of this magical material by several orders of magnitude, from the condition of almost compensated donors and acceptors (nearly insulating state) to a highly conducting n-type material. It is important to point out once again that the aforementioned connection between the defect states, photoluminescence, and photoresponse is borne out fairly well by the systematic reflected in Figure 9C.

4. CONCLUSION

We report a dramatic enhancement of the photoresponse in hydrothermally grown faceted β-In_2S_3 films through fine synthetic control of the equilibrium between donor- and acceptor-type defect states, which leads to strong suppression of dark conductivity through carrier compensation. The highest photoresponse, i.e., $\sim 10^4$ times, is obtained for the film synthesized for 10 h through hydrothermal processing. Detailed characterizations performed with multiple techniques, and the analyses of the corresponding data, elucidate the key role of the defect states and their electronic consequences for transport properties in this rather intriguing material system.

■ ASSOCIATED CONTENT

Ⓢ Supporting Information

This material is available free of charge via the Internet at http://pubs.acs.org/. The Supporting Information is available free of charge on the ACS Publications website at DOI: 10.1021/acsami.5b02885.

Figure SI-1 gives the XRD patterns of FTO substrate and films through hydrothermal reactions over time. SI-2 presents the time dependent variation in highest intensity XRD peaks. SI-3A gives FESEM images of the film grown on FTO substrates over time. SI-3B shows the schematic presentation of growth evolution leading to the formation of In_2S_3 octahedrons. SI-4 shows the $I-V$ curves in thedark and under illumination for photodetector devices. SI-5 presents the rise and reset time data for H_{10}-In_2S_3 and S-In_2S_3. SI-6 presents the photocurrent data for the FTO-In_2S_3-ITO device as a function of incident optical power and related calculations of photoconductive gain. (PDF)

■ AUTHOR INFORMATION

Corresponding Authors

*E-mail: nilima.chaudhari07@gmail.com.
*E-mail: sandesh@physics.unipune.ac.in.
*E-mail: sb.ogale@ncl.res.in, satishogale@gmail.com. Tel.: +91 20 25902260; Fax: +91 20 25902260, 020 25691684.

Notes

The authors declare no competing financial interest.

■ ACKNOWLEDGMENTS

Nilima S. Chaudhari gratefully acknowledges financial support from UGC India under the award of a Dr. D. S. Kothari postdoctoral fellowship.

■ REFERENCES

(1) Rehwald, W.; Harbeke, G. On the Conduction Mechanism in Single Crystal β-Indium Sulfide In_2S_3. *J. Phys. Chem. Solids* **1965**, *26*, 1309−1318.

(2) Hong, J. W.; Lee, S. U.; Lee, Y. W.; Han, S. W. Hexoctahedral Au Nanocrystals with High-Index Facets and Their Optical and Surface-Enhanced Raman Scattering Properties. *J. Am. Chem. Soc.* **2012**, *134*, 4565−4568.

(3) Naik, S. D.; Jagdale, T. C.; Apte, S. K.; Sonawane, R. S.; Kulkarni, M. V.; Patil, S. I.; Ogale, S. B.; Kale, B. B. Rapid Phase-Controlled Microwave Synthesis of Nanostructured Hierarchical Tetragonal and Cubic β-In_2S_3 Dandelion Flowers. *Chem. Phys. Lett.* **2008**, *452*, 301−305.

(4) Liu, L.; Liu, H.; Kou, H. Z.; Wang, Y.; Zhou, Z.; Ren, M.; Ge, M.; He, X. Morphology Control of β-In_2S_3 from Chrysanthemum-Like Microspheres to Hollow Microspheres: Synthesis and Electrochemical Properties. *Cryst. Growth Des.* **2009**, *9*, 113−117.

(5) Nagesha, D. K.; Liang, X.; Mamedov, A. A.; Gainer, G.; Eastman, M. A.; Giersig, M.; Song, J. J.; Ni, T.; Kotov, N. A. In_2S_3 Nanocolloids with Excitonic Emission: In_2S_3 vs CdS Comparative Study of Optical and Structural Characteristics. *J. Phys. Chem. B* **2001**, *105*, 7490−7498.

(6) Xing, Y.; Zhang, H.; Song, S.; Feng, J.; Lei, Y.; Zhao, L.; Li, M. Hydrothermal Synthesis and Photoluminescent Properties of Stacked Indium Sulfide Superstructures. *Chem. Commun.* **2008**, 1476−1478.

(7) Dalas, E.; Kobotiatis, L. Primary Solid-State Batteries Constructed from Copper and Indium Sulphides. *J. Mater. Sci.* **1993**, *28*, 6595−6597.

(8) Kim, Y. H.; Lee, J. H.; Shin, D. W.; Park, S. M.; Moon, J. S.; Nam, J. G.; Yoo, J. B. Synthesis of Shape-Controlled β-In_2S_3 Nanotubes through Oriented Attachment of Nanoparticles. *Chem. Commun.* **2010**, *46*, 2292−2294.

(9) Datta, A.; Sinha, G.; Panda, S. K.; Patra, A. Growth, Optical, and Electrical Properties of In_2S_3 Zigzag Nanowires. *Cryst. Growth Des.* **2009**, *9*, 427−431.

(10) Cansizoglu, H.; Cansizoglu, M. F.; Finckenor, M.; Karabacak, T. Optical Absorption Properties of Semiconducting Nanostructures with Different Shapes. *Adv. Opt. Mater.* **2013**, *1*, 158−166.

(11) Cansizoglu, M. F.; Engelken, R.; Seo, H. W.; Karabacak, T. High Optical Absorption of Indium Sulfide Nanorod Arrays Formed by Glancing Angle Deposition. *ACS Nano* **2010**, *4*, 733−740.

(12) Acharya, S.; Dutta, M.; Sarkar, S.; Basak, D.; Chakraborty, S.; Pradhan, N. Synthesis of Micrometer Length Indium Sulfide Nanosheets and Study of Their Dopant Induced Photoresponse Properties. *Chem. Mater.* **2012**, *24*, 1779−1785.

(13) Tang, J.; Konstantatos, G.; Hinds, S.; Myrskog, S.; Pattantyus-Abraham, A. G.; Clifford, J.; Sargent, E. H. Heavy-Metal-Free Solution-Processed Nanoparticle-Based Photodetectors: Doping of Intrinsic Vacancies Enables Engineering of Sensitivity and Speed. *ACS Nano* **2009**, *3*, 331−338.

(14) Bareau, N.; Bernede, J. C.; Maliki, H. E.; Marsillac, S.; Castel, X.; Pinel, J. Recent Studies on In_2S_3 containing Oxygen Thin Films. *Solid State Commun.* **2002**, *122*, 445−450.

(15) Cansizoglu, H.; Cansizoglu, M. F.; Watanabe, F.; Karabacak, T. Enhanced Photocurrent and Dynamic Response in Vertically Aligned In_2S_3/Ag Core/Shell Nanorod Array Photoconductive Devices. *ACS Appl. Mater. Interfaces* **2014**, *6*, 8673−8682.

(16) Peng, S.; Zhu, P.; Thavasi, V.; Mhaisalkar, S. G.; Ramakrishna, S. Facile Solution Deposition of $ZnIn_2S_4$ Nanosheet Films on FTO Substrates for Photoelectric Application. *Nanoscale* **2011**, *3*, 2602−2608.

(17) Mandal, L.; Chaudhari, N. S.; Ogale, S. Self-Powered UV-vis Photodetector Based on $ZnIn_2S_4$/Hydrogel Interface. *ACS Appl. Mater. Interfaces* **2013**, *5*, 9141−9147.

(18) Gu, Y.; Xu, Z.; Guo, L.; Wan, Y. ZnO Nanoplate-Induced Phase Transformation Synthesis of the Composite ZnS/$In(OH)_3$/In_2S_3 with Enhanced Visible-Light Photodegradation Activity of Pollutants. *CrystEngComm* **2014**, *16*, 10997−11006.

(19) Li, Z.; Dong, T.; Zhang, Y.; Wu, L.; Li, J.; Wang, X.; Fu, X. Studies on $In(OH)_yS_z$ Solid Solutions: Syntheses, Characterizations, Electronic Structure, and Visible-Light-Driven Photocatalytic Activities. *J. Phys. Chem. C* **2007**, *111*, 4727−4733.

(20) Wu, J.; Liu, L.; Liu, S.; Yu, P.; Zheng, Z.; Shafa, M.; Zhou, Z.; Li, H.; Ji, H.; Wang, Z. M. High Responsivity Photoconductors Based on Iron Pyrite Nanowires Using Sulfurization of Anodized Iron Oxide Nanotubes. *Nano Lett.* **2014**, *14*, 6002−6009.

(21) Banerjee, A.; Upadhyay, K. K.; Bhatnagar, S.; Tathavadekar, M.; Bansode, U.; Agarkar, S.; Ogale, S. B. Nickel Cobalt Sulfide Nanoneedle Array as an Effective Alternative to Pt as a Counter Electrode in Dye Sensitized Solar Cells. *RSC Adv.* **2014**, *4*, 8289−8294.

(22) Faur, M.; Faur, M.; Jayne, D. T.; Goradia, M.; Goradia, C. XPS Investigation of Anodic Oxides Grown on p-type InP. *Surf. Interface Anal.* **1990**, *15*, 641−650.

(23) Li, C. P.; Hercules, D. M. A Surface Spectroscopic Study of Sulfided Molybdena-Alumina Catalysts. *J. Phys. Chem.* **1984**, *88*, 456−464.

(24) Biswas, P. K.; De, A.; Dua, L. K.; Chkada, A. L. Surface Characterization of Sol- Gel Derived Indium Tin Oxide Films on Glass. *Bull. Mater. Sci.* **2006**, *29*, 323−330.

(25) Zhao, Y.; Dong, G.; Duan, L.; Qiao, J.; Zhang, D.; Wang, L.; Qiu, Y. Impacts of Sn Precursors on Solution-processed Amorphous Zinc−Tin Oxide Films and Their Transistors. *RSC Adv.* **2012**, *2*, 5307−5313.

(26) Simonsen, M. E.; Sonderby, C.; Li, Z.; Sogaard; Erik, G. XPS and FT-IR Investigation of Silicate Polymers. *J. Mater. Sci.* **2009**, *44*, 2079−2088.

(27) Naik, B.; Parida, K. M.; Gopinath, C. S. Facile Synthesis of N- and S-Incorporated Nanocrystalline TiO_2 and Direct Solar-Light-Driven Photocatalytic Activity. *J. Phys. Chem. C* **2010**, *114*, 19473−19482.

(28) Chaudhari, N. S.; Warule, S. S.; Muduli, S.; Kale, B. B.; Jouen, S.; Lefez, B.; Hannoyer, B.; Ogale, S. B. Maghemite (Hematite) Core (Shell) Nanorods *via* Thermolysis of a Molecular Solid of Fe-complex. *Dalton Trans.* **2011**, *40*, 8003−8011.

(29) Akbarzadeh, R.; Dehghani, H.; Behnoudnia, F. Sodium Thiosulfate-Assisted Synthesis of NiS_2 Nanostructure by Using Nickel(II)-Salen Precursor: Optical and Magnetic Properties. *Dalton Trans.* **2014**, *43*, 16745−16753.

(30) Yamaguchi, T.; Jin, T.; Tanabe, K. Structure of Acid Sites on Sulfur-Promoted Iron Oxide. *J. Phys. Chem.* **1986**, *90*, 3148−3152.

(31) Iyengar, R. R.; Sathyanarayana, D. N.; Patel, C. C. Thioacetamide Complexes of Nickel(II) and Copper(I) Chlorides. *J. Inorg. Nucl. Chem.* **1972**, *34*, 1088−1091.

(32) Yan, T.; Long, J.; Shi, X.; Wang, D.; Li, Z.; Wang, X. Efficient Photocatalytic Degradation of Volatile Organic Compounds by Porous Indium Hydroxide Nanocrystals. *Environ. Sci. Technol.* **2010**, *44*, 1380−1385.

(33) Mandal, L.; Deo, M.; Yengantiwar, A.; Banpurkar, A.; Jog, J.; Ogale, S. A Quasi-Liquid Iontronic−Electronic Light-Harvesting Hybrid Photodetector with Giant Response. *Adv. Mater.* **2012**, *24*, 3686−3691.

(34) Menon, R.; Mancini, A.; Sudha Kartha, C.; Vijayakumar, K. P.; Santoni, A. Band Offset of the In_2S_3/Indium Tin Oxide Interface Measured by X-ray Photoelectron Spectroscopy. *Thin Solid Films* **2012**, *520*, 5856−5859.

(35) Shifu, C.; Xiaoling, Y.; Huaye, Z.; Wei, L. Preparation, Characterization and Activity Evaluation of Heterostructure In_2O_3/$In(OH)_3$ Photocatalyst. *J. Hazard. Mater.* **2010**, *180*, 735−740.

(36) Jayakrishnan, R.; John, T. T.; Kartha, C. S.; Vijayakumar, K. P.; Abe, T.; Kashiwaba, Y. Defect Analysis of Sprayed β-In_2S_3 Thin Films Using Photoluminescence Studies. *Semicond. Sci. Technol.* **2005**, *20*, 1162−1167.

(37) Joffe, A. Properties of Various Semiconductors. *J. Phys. Chem. Solids* **1959**, *8*, 6−13.